c-axis oriented epitaxial $BaTiO_3$ films on (001) Si

V. Vaithyanathan,[a),b)] J. Lettieri,[c)] W. Tian,[a)] A. Sharan, A. Vasudevarao, and Y. L. Li[d)]
Department of Materials Science and Engineering, Penn State University, University Park, Pennsylvania 16802–5005

A. Kochhar,[a)] H. Ma,[a)] and J. Levy[a)]
Department of Physics and Astonomy, University of Pittsburgh, Pittsburgh, Pennsylvania 15260

P. Zschack
University of Illinois, APS-UNICAT, Argonne National Lab, Argonne, Illinois 60439

J. C. Woicik
National Institute of Standards and Technology, Gaithersburg, Maryland 20899

L. Q. Chen, V. Gopalan, and D. G. Schlom[a),e)]
Department of Materials Science and Engineering, Penn State University, University Park, Pennsylvania 16802–5005

(Received 29 October 2005; accepted 10 April 2006; published online 27 July 2006)

c-axis oriented epitaxial films of the ferroelectric $BaTiO_3$ have been grown on (001) Si by reactive molecular-beam epitaxy. The orientation relationship between the film and substrate is (001) $BaTiO_3 \parallel (001)$ Si and [100] $BaTiO_3 \parallel [110]$ Si. The uniqueness of this integration is that the entire epitaxial $BaTiO_3$ film on (001) Si is *c*-axis oriented, unlike any reported so far in the literature. The thermal expansion incompatibility between $BaTiO_3$ and silicon is overcome by introducing a relaxed buffer layer of $Ba_xSr_{1-x}TiO_3$ between the $BaTiO_3$ film and silicon substrate. The rocking curve widths of the $BaTiO_3$ films are as narrow as 0.4°. X-ray diffraction and second harmonic generation experiments reveal the *out-of-plane* *c*-axis orientation of the epitaxial $BaTiO_3$ film. Piezoresponse atomic force microscopy is used to write ferroelectric domains with a spatial resolution of ~100 nm, corroborating the orientation of the ferroelectric film. © *2006 American Institute of Physics*. [DOI: 10.1063/1.2203208]

I. INTRODUCTION

The reorientable dielectric polarization offered by a ferroelectric material is a critical element of a number of current and emerging device structures. Epitaxial ferroelectric films offer a means to constrain the possible directions in which the spontaneous polarization can exist and thus can offer significant performance advantages over randomly oriented ferroelectric films, provided they restrict the polarization to lie in directions desired for the particular application. Depending on the application of interest, polarization entirely in-plane or entirely out-of-plane is often optimal.

$BaTiO_3$ and related materials are used in many devices exploiting the dielectric,[1] pyroelectric,[2] piezoelectric,[3] electrostrictive,[4] ferroelectric,[5] electro-optic,[6,7] and nonlinear optical[8] characteristics of this material. The successful integration of epitaxial $BaTiO_3$ with an extensively used semiconductor such as silicon would offer functionalities (not found in conventional semiconductors) to be utilized in silicon-based semiconductor electronics.

Epitaxial $BaTiO_3$ films have been grown on silicon with a buffer layer between the film and the silicon substrate,[9–13] and all such reported epitaxial $BaTiO_3$ films on silicon possess an *in-plane* polarization. This arises for two reasons. First, the lattice mismatch $[(a_{sub}-a_{film})/a_{film}$, where a_{sub} is the lattice constant of the substrate and a_{film} is the lattice constant of the film$]$[14] between $BaTiO_3$ and (001) Si is large, −4.5% at growth temperature (~600 °C).[15,16] With such a large lattice mismatch, the resulting $BaTiO_3$ films are relaxed during growth by the introduction of misfit dislocations, even for a film thickness of only a few unit cells. Second, due to the much smaller thermal expansion coefficient of silicon as compared to $BaTiO_3$,[15,16] the relaxed $BaTiO_3$ films end up in a state of biaxial tension as they are cooled through the Curie temperature (130 °C for unstrained $BaTiO_3$).[17] To relieve this biaxial tensile strain state, the tetragonal $BaTiO_3$ films orient with their longer axis (*c*-axis) in the plane of the substrate and their shorter axis (*a*-axis) oriented out-of-plane. This results in an in-plane polarization of the $BaTiO_3$ film because the dielectric polarization lies along the *c*-axis of tetragonal $BaTiO_3$. Although the in-plane polarization is suitable for some applications,[18,19] there are many applications in which an out-of-plane polarization of the $BaTiO_3$ ferroelectric layer is desired. These include ferroelectric memory devices,[20] which require top and bottom electrodes, as well as a quantum computing architecture in which spin interactions in the underlying silicon are controlled by the out-of-plane polarization of an overlying ferroelectric film.[21] The

[a)]Also at Center for Oxide-Semiconductor Materials for Quantum Computation (COSMQC), University of Pittsburgh, Pittsburgh, Pennsylvania 15260
[b)]Present address: Seagate Technology, Pittsburgh, PA 15222.
[c)]Deceased.
[d)]Present address: MST-STC, Los Alamos National Laboratory, Los Alamos, NM 87544
[e)]Electronic mail: schlom@ems.psu.edu

 © 2006 American Institute of Physics

Downloaded 05 Apr 2007 to 128.118.88.141. Redistribution subject to AIP license or copyright, see http://jap.aip.org/jap/copyright.jsp

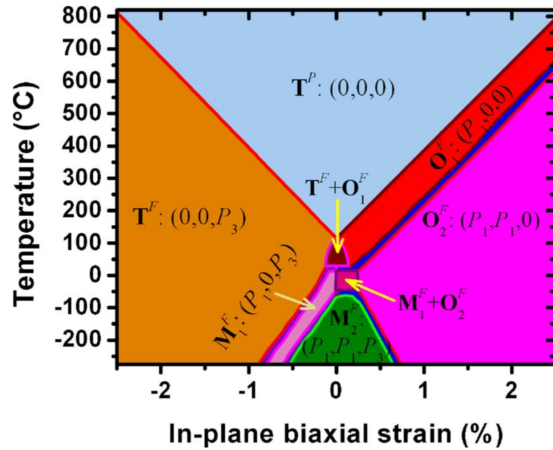

FIG. 1. (Color online) Stability phase diagram for epitaxial {100} oriented $BaTiO_3$ thin films as a function of temperature and total in-plane biaxial strain (resulting from lattice mismatch and thermal expansion mismatch), predicted using phase-field simulations. Positive strain values are for films in a biaxial tensile strain state while negative strain values are for films in a biaxial compressive strain state. The letters **T**, **O**, and **M** used in the phase notations indicate tetragonal, orthorhombic, and monoclinic crystallographic symmetries, respectively, under a constraint. The paraelectric and ferroelectric natures of the phases are revealed by the superscript *P* and *F*, respectively. $\mathbf{M}_1^F+\mathbf{O}_2^F$ implies a mixture of $\mathbf{M}_1^F$ and $\mathbf{O}_2^F$ phases. The components of the polarization vector $\boldsymbol{P}$ corresponding to the phases (along the crystallographic directions of the pseudocubic $BaTiO_3$) are indicated within the parentheses following the phase notation.

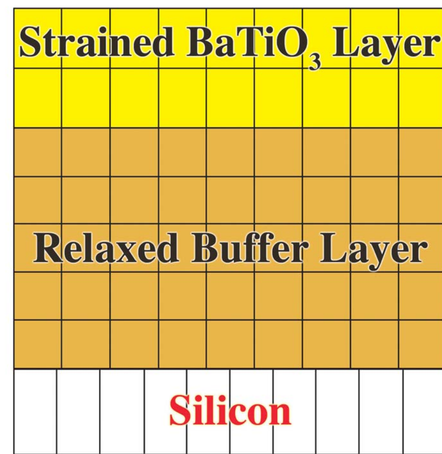

FIG. 2. (Color online) A schematic of the structure used for the growth of epitaxial *c*-axis $BaTiO_3$ on Si (001). The structure involves the presence of a completely relaxed buffer layer between the silicon and the ferroelectric $BaTiO_3$. The thickness of the epitaxial $BaTiO_3$ should be below its critical thickness.

influence of strain, arising, for example, from lattice mismatch in conjunction with thermal expansion mismatch, on the orientation of the spontaneous polarization axis in thin ferroelectric films is well established.[22–26] Figure 1 displays the stability of various ferroelectric phases and domain structures in {100} oriented $BaTiO_3$ thin films as a function of temperature and biaxial strain. The temperature-strain stability diagram was constructed using phase-field simulations in which an eighth-order Landau-Devonshire thermodynamic potential was employed for describing the bulk free energy of $BaTiO_3$.[25,26] From Fig. 1, it is evident that by tailoring the total strain (lattice mismatch and thermal expansion mismatch) between the film and the substrate, the resulting orientation of a $BaTiO_3$ film can be varied from a purely *a*-axis oriented (where the *a*-axis lies perpendicular to the plane of the substrate), to a mixture of *c* and *a* axes oriented, to purely *c*-axis oriented (where the *c*-axis lies perpendicular to the plane of the substrate).[22,24–27] Large biaxial tensile strain results in *a*-axis films, while large biaxial compressive strain results in *c*-axis films.[23,26]

II. HETEROSTRUCTURE STRATEGY

Orientation control is achieved in this work by incorporating a buffer layer between the $BaTiO_3$ film and silicon substrate. The use of buffer layers for growing $BaTiO_3$ on Si (001) is not a new concept.[9–12,28] McKee and Walker grew the $BaTiO_3$ on silicon with either buffer layers that are lattice matched to the silicon (e.g., $Ba_{0.725}Sr_{0.275}O$ and $Ca_{0.64}Sr_{0.36}TiO_3$) (Ref. 29) or compositionally graded $Ba_xSr_{1-x}TiO_3$ buffer layers.[30] The resulting films were *a*-axis oriented because the $BaTiO_3$ layer was sufficiently relaxed at growth temperature, and was subjected to a state of biaxial tension (from the comparatively smaller thermal expansion coefficient of the silicon substrate) as it was cooled through its Curie temperature. Nonetheless, by patterning the film into small islands, these authors succeeded in making local *c*-axis oriented regions (55 μm or less in extent) at the outer edge of the $BaTiO_3$ islands in otherwise *a*-axis oriented $BaTiO_3$ films on silicon.[29]

In this work, we have used buffer layers to render an entire $BaTiO_3$ film on silicon *c*-axis oriented, without the need for patterning into tiny islands. The important requirements of such a buffer layer are the following. First, the buffer layer should enable the epitaxial growth of a *commensurate* $BaTiO_3$ overlayer. The lattice mismatch between the buffer layer and the $BaTiO_3$ should be sufficiently small to enable the growth of a commensurate $BaTiO_3$ overlayer of the required thickness. Second, the biaxial compressive strain in such a commensurate $BaTiO_3$ film needs to be sufficient to overcome (by at least -0.1% to -0.2%) (Ref. 26) the thermal expansion mismatch-induced biaxial tensile strain (+0.4%) that arises during cooling from the growth temperature. Satisfying this criterion will result in the spontaneous polarization orienting *out-of-plane* as the $BaTiO_3$ film is cooled through its Curie temperature (according to Fig. 1). Third, the buffer layer thickness should greatly exceed the critical thickness for the onset of relaxation, as a completely relaxed buffer layer is desired. Finally, should the buffer layer exhibit any ferroelectric transitions, they should occur below the Curie temperature of the compressively strained $BaTiO_3$ film. A schematic of the proposed structure to stabilize a *c*-axis oriented $BaTiO_3$ on Si (001) is shown in Fig. 2.

III. CRITICAL THICKNESS ANALYSIS

A buffer layer satisfying these requirements is a solid solution of barium and strontium titanate ($Ba_xSr_{1-x}TiO_3$), with a lattice parameter that can be varied with its composition. $Ba_xSr_{1-x}TiO_3$ with a composition of $x=0.7$ and a lattice

Downloaded 05 Apr 2007 to 128.118.88.141. Redistribution subject to AIP license or copyright, see http://jap.aip.org/jap/copyright.jsp

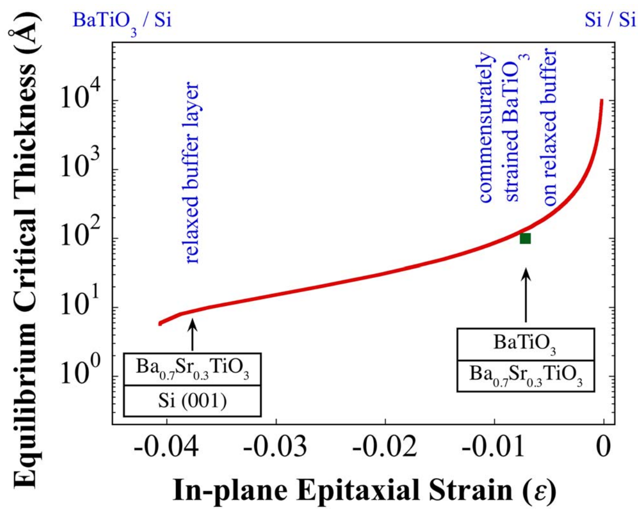

FIG. 3. (Color online) Theoretical equilibrium critical thickness estimated using Matthews-Blakeslee analysis [Eq. (1)] for a $BaTiO_3$ film at 600 °C, as a function of the in-plane epitaxial strain in the film. The square data point indicates the typical thickness of the strained $BaTiO_3$ film (~100 Å) required on top of the fully relaxed buffer layer on Si (001) for the quantum computing application of interest.

parameter of about 4.00 Å (assuming Vegard's law[31,32]) at the growth temperature (~600 °C) was used as the buffer layer in this study.[15,16]

The composition of the buffer layer and its thickness were chosen based on an analysis made using the Matthews-Blakeslee equation for the equilibrium critical thickness,[14,33,34]

$$\varepsilon = \frac{b}{8\pi h_c}\frac{(1-\nu\cos^2\alpha)}{(1+\nu)\cos\lambda}\left[\ln\left(\frac{h_c}{b}\right)+1\right], \qquad (1)$$

where ε is the lattice misfit between the film and the substrate, h_c is the equilibrium critical thickness of the film, b is the Burgers vector of the dislocations relaxing the film, ν is the Poisson ratio of the film, α is the angle between the dislocation line and its Burgers vector, and λ is the angle between the slip direction and the direction in the film plane, which is perpendicular to the line of intersection of the slip plane and the interface. Knowledge of the slip system involved in producing the misfit dislocations is required to apply this model effectively. Based on the work of Suzuki *et al.*[35] the parameters b, α, and λ in Eq. (1) are $a\langle 100\rangle$ (where a is the lattice constant of cubic $BaTiO_3$ at a growth temperature of 600 °C),[15] 90°, and 45°, respectively. The Poisson ratio ($\nu=-s_{12}/s_{11}$, where s_{11} and s_{12} are compliance tensor elements) was taken to be 0.385 from elastic constant measurements of cubic $BaTiO_3$ at 150 °C (the highest temperature at which these tensor elements have been reported).[36] The critical thickness versus epitaxial strain plot obtained from Eq. (1) for $BaTiO_3$ is shown in Fig. 3.

Assuming that $Ba_xSr_{1-x}TiO_3$ and $BaTiO_3$ thin films are similar in nature, we apply the critical thickness plot in Fig. 1 to films of both materials. At a composition of x=0.7, the strain between the $Ba_xSr_{1-x}TiO_3$ buffer layer and silicon ($\varepsilon=-3.77\%$ at T_{sub}=600 °C)[15,16,31,32] implies an equilibrium critical thickness (h_c) of ~10 Å. While h_c is the thickness at which it becomes energetically favorable for the relaxation of the epitaxial film to begin, complete relaxation is not expected until the film is considerably thicker. This thickness is dependent on kinetic factors,[37] but a buffer layer thickness several times thicker than the equilibrium critical thickness can be anticipated to ensure its complete relaxation (i.e., a minimum buffer layer thickness of several tens of angstroms).

The strain between such a relaxed buffer layer and an overgrown $BaTiO_3$ film should be small enough to enable the growth of a commensurately strained $BaTiO_3$ film of the desired thickness for the specific application. For our application, a commensurately strained $BaTiO_3$ film of about 100 Å thick is desired (square data point in Fig. 3). At the growth temperature (~600 °C), the biaxial compressive strain state in such a commensurate $BaTiO_3$ film should be $\varepsilon=-0.7\%$.[15,16] Upon cooling to room temperature, this will decrease to a biaxial compressive strain of $\varepsilon=-0.3\%$ due to the thermal expansion mismatch between $BaTiO_3$ and Si [$\varepsilon=+0.4\%$ (Ref. 38) arising from the thermal expansion mismatch].[15,16] From Fig. 1, this small compressive strain should be sufficient to achieve purely c-axis oriented $BaTiO_3$.

IV. GROWTH PROCEDURE

The films used in this study were grown by reactive molecular-beam epitaxy (MBE) from elemental sources in an EPI 930 MBE system modified for the growth of oxides. A complete description of the system can be found elsewhere.[39–41] The process used to grow an epitaxial perovskite layer on (001) Si is a modification[39–41] of the method developed by Walker and co-workers.[11,29,30,42,43] The oxygen pressures used at various steps in the growth are based on extensive oxidation studies, which determine the minimum oxygen partial pressure necessary to oxidize the depositing species.[44] Substrate temperatures below 550 °C are based on measurements from a thermocouple near, but not in contact with the substrate. Temperatures above 550 °C are measured using an optical pyrometer (assuming an emissivity of 0.8 for the substrate). The difference between the real temperature and the thermocouple temperature at a real temperature of 600 °C (by pyrometer) is ~75–100 °C and the difference decreases as the temperature is lowered. The crystallinity of the film surface was monitored *in situ* during growth using reflection high-energy electron diffraction (RHEED).

The $BaTiO_3/Ba_xSr_{1-x}TiO_3$/Si (001) epitaxial films were grown using the following steps. Before loading into the MBE chamber, the (001) Si wafers were exposed to UV light from a mercury lamp with a quartz bulb for 15–20 min to remove surface organics by the ozone produced by the UV light. After loading into the MBE chamber, which has a base pressure of $(2-3)\times 10^{-9}$ Torr, the wafers were heated to ~980 °C to desorb the native SiO_2 layer. RHEED then revealed a double-domain (2×1) reconstruction as shown in Fig. 4(a). The substrate was then cooled to 700 °C where the clean Si surface was exposed to 1/2 monolayer[45] (ML) of strontium (strontium flux, $J_{Sr}\sim 1.4\times 10^{13}$ atoms $cm^{-2}\,s^{-1}$) to form strontium silicide ($SrSi_x$). During this step, the RHEED pattern dynamically

Downloaded 05 Apr 2007 to 128.118.88.141. Redistribution subject to AIP license or copyright, see http://jap.aip.org/jap/copyright.jsp

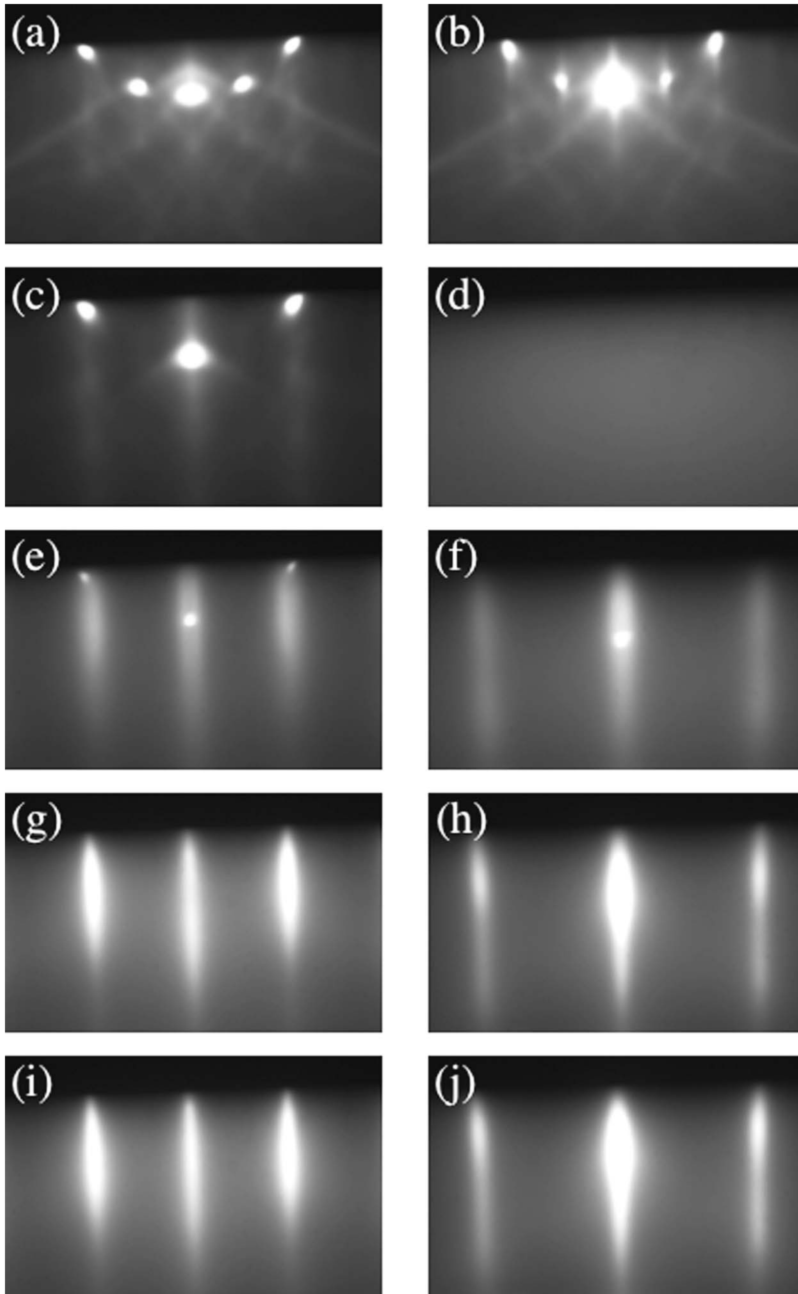

FIG. 4. RHEED patterns along the [110] azimuth of Si from different stages of growth of the 100 Å $BaTiO_3$/300 Å $Ba_{0.7}Sr_{0.3}TiO_3$/(001) Si heterostructure. (a) 2× reconstructed silicon surface after desorbing the SiO_2 at 980 °C, (b) after the deposition of 1/2 ML Sr to form $SrSi_x$ at 700 °C, (c) after the deposition of 3 ML of $Ba_{0.7}Sr_{0.3}O$ at ~100 °C, and (d) after the deposition of 2 ML of amorphous TiO_2 at ~100 °C. (e) and (f) RHEED patterns after recrystallization of 2 unit cells of $Ba_{0.7}Sr_{0.3}TiO_3$, viewed along the [110] and [100] azimuths of silicon, respectively. (g) and (h) RHEED patterns after the growth of a 300-Å-thick $Ba_{0.7}Sr_{0.3}TiO_3$ buffer layer along the [110] and [100] azimuths of silicon, respectively. (i) and (j) RHEED patterns along the [110] and [100] azimuths of silicon, respectively, following the growth of the 100 Å of $BaTiO_3$ completing the heterostructure.

reflects the changes in the silicide layer through a series of reconstructions.[39] The RHEED pattern of 1/2 ML $SrSi_x$ has a 2× reconstruction, as shown in Fig. 4(b). This silicide template has been shown to be comparatively robust to oxygen exposure and to resist the formation of amorphous SiO_2.[46] The substrate was then cooled to ~100 °C for the deposition of a 1/2 ML of $Ba_{0.7}Sr_{0.3}$ metal with $J_{Ba} \sim 3.3 \times 10^{13}$ and $J_{Sr} \sim 1.4 \times 10^{13}$ atoms cm^{-2} s^{-1}. Oxygen was then introduced to a background pressure of 4×10^{-8} Torr during which an additional 2.5 ML of $Ba_{0.7}Sr_{0.3}$ was deposited to form a total of 3 ML of epitaxial $Ba_{0.7}Sr_{0.3}O$ (the underlying 1/2 ML of $Ba_{0.7}Sr_{0.3}$ also gets oxidized during this step). The 3-ML-thick epitaxial $Ba_{0.7}Sr_{0.3}O$ film so formed is commensurately strained with the substrate, as revealed by the spots on an arc in the RHEED pattern in Fig. 4(c).[47,48] This was followed by the deposition of 2 ML of titanium ($J_{Ti} \sim 4 \times 10^{13}$ atoms cm^2 s) in a background oxygen partial pressure of 2×10^{-7} Torr to form 2 ML of amorphous TiO_2 [shown in Fig. 4(d)].

The wafer was then heated in UHV ((1–2) $\times 10^{-9}$ Torr) to ~550 °C to enable the recrystallization of the perovskite $Ba_{0.7}Sr_{0.3}TiO_3$ through a topotactic reaction that occurs as the 2 MLs of TiO_2 diffuse into the underlying 3 MLs of $Ba_{0.7}Sr_{0.3}O$ to form 2 unit cells of $Ba_{0.7}Sr_{0.3}TiO_3$.[41,49] The RHEED pattern of the recrystallized epitaxial $Ba_{0.7}Sr_{0.3}TiO_3$ is shown in Figs. 4(e) and 4(f), along the [110] and [100] azimuths of silicon, respectively. The streaky nature of the RHEED pattern of $Ba_{0.7}Sr_{0.3}TiO_3$ in Fig. 4(e) indicates that the layer is partially relaxed even for a thickness of 2 unit cells.[50] Further growth of the remaining buffer layer of epitaxial $Ba_{0.7}Sr_{0.3}TiO_3$ was achieved by shuttered growth[51] (involving the supply of alternate monolayer

Downloaded 05 Apr 2007 to 128.118.88.141. Redistribution subject to AIP license or copyright, see http://jap.aip.org/jap/copyright.jsp

doses of $Ba_{0.7}Sr_{0.3}$ and titanium) at a substrate temperature of 550–570 °C in an oxygen background pressure of (4–5) $\times 10^{-8}$ Torr. In order to ensure that the $Ba_{0.7}Sr_{0.3}TiO_3$ buffer layer was completely relaxed, a 300-Å-thick buffer layer (75 unit cells) was grown. The RHEED patterns of a 300-Å-thick $Ba_{0.7}Sr_{0.3}TiO_3$ buffer layer along the [110] and [100] azimuths of silicon are shown in Figs. 4(g) and 4(h), respectively.

It can be seen from Fig. 3 that the equilibrium critical thickness (energetically favorable thickness for the onset of relaxation) for the $Ba_{0.7}Sr_{0.3}TiO_3$ buffer layer on silicon is ~10 Å. Though the results shown here are for a buffer layer thickness of 300 Å, we have investigated different buffer layer thicknesses from 40 to 300 Å. Based on the x-ray diffraction (XRD) analyses of these films (details discussed below in the XRD section), it can be inferred qualitatively that the minimum thickness of the $Ba_{0.7}Sr_{0.3}TiO_3$ buffer layer for complete relaxation is ~100 Å. Complete relaxation of the $Ba_{0.7}Sr_{0.3}TiO_3$ buffer layer is necessary to strain a commensurate overlying $BaTiO_3$ film sufficiently to make it pure *c*-axis oriented after cooling to room temperature.

On top of the 300-Å-thick $Ba_{0.7}Sr_{0.3}TiO_3$ buffer layer, a 100-Å-thick $BaTiO_3$ layer was grown using the same growth temperature and oxygen partial pressure as the $Ba_{0.7}Sr_{0.3}TiO_3$ buffer layer. The RHEED patterns of the 100-Å-thick $BaTiO_3$ film in Figs. 4(i) and 4(j) were obtained along the [110] and [100] azimuths of silicon, respectively.

V. X-RAY DIFFRACTION

The structural quality of the film was assessed *ex situ* using a four-circle x-ray diffractometer with a Cu $K\alpha$ source ($\lambda \sim 1.54$ Å). Figure 5(a) shows a θ-2θ scan of the 100 Å $BaTiO_3$/300 Å $Ba_{0.7}Sr_{0.3}TiO_3$/Si(001) film in which the 00ℓ peaks of the $BaTiO_3$ and $Ba_{0.7}Sr_{0.3}TiO_3$ (indistinguishable at low angles because of the small difference in lattice parameters) are labeled. The good structural quality of the film is revealed by the narrow rocking curve (ω-scan) full width at half maximum (FWHM) of 0.38° of the 002 peak. The out-of-plane lattice parameters of the $Ba_{0.7}Sr_{0.3}TiO_3$ and $BaTiO_3$ film obtained from a scan of the 004 peaks[52] [shown in Fig. 5(b)], are 3.960±0.001 and 4.025±0.003 Å (error bars based on a Gaussian fit), respectively, indicating that the entire $BaTiO_3$ film is *c*-axis oriented. A ϕ-scan of the 111 $Ba_{0.7}Sr_{0.3}TiO_3/BaTiO_3$ peak (FWHM in ϕ of 1.65°), in Fig. 5(c) reveals the epitaxial nature of the buffer layer and film. The epitaxial relationship of the film to the substrate is (001) $BaTiO_3 \parallel$ (001) Si and [100] $BaTiO_3 \parallel$ [110] Si.

The out-of-plane lattice constant of the $Ba_{0.7}Sr_{0.3}TiO_3$ and $BaTiO_3$ layers obtained using the 004 peak positions can be used to assess qualitatively the extent of relaxation of the $Ba_{0.7}Sr_{0.3}TiO_3$ buffer layer and the in-plane strain state of the $BaTiO_3$ layer. Using such an analysis on heterostructures with 80–100 Å-thick $BaTiO_3$ layers on top of $Ba_{0.7}Sr_{0.3}TiO_3$ buffer layers with thickness varying from 40–300 Å on Si (001), we estimate that the thickness of the $Ba_{0.7}Sr_{0.3}TiO_3$ buffer layer should be at least 100 Å for its complete relaxation. The x-ray 004 peaks of $Ba_{0.7}Sr_{0.3}TiO_3$ and $BaTiO_3$ as a function of $Ba_{0.7}Sr_{0.3}TiO_3$ buffer layer thickness are shown

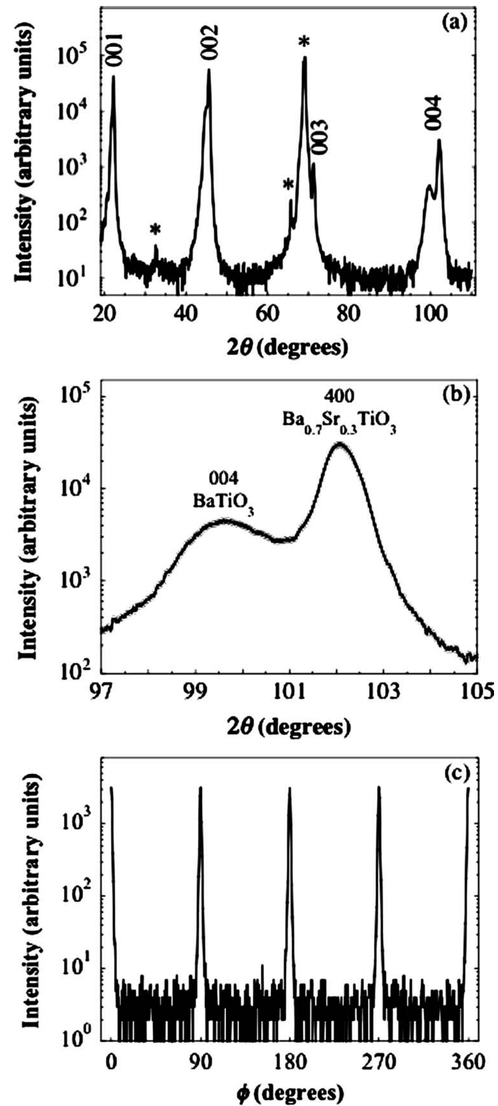

FIG. 5. (a) θ-2θ scan of the same 100 Å $BaTiO_3$/300 Å $Ba_{0.7}Sr_{0.3}TiO_3$/Si (001) heterostructure whose RHEED patterns are shown in Fig. 4, showing the 00ℓ peaks of $BaTiO_3$ and $Ba_{0.7}Sr_{0.3}TiO_3$. The FWHM of the 002 peak in 2θ and ω are 0.42° and 0.38°, respectively. The Si 004 substrate peak and other peaks ($\lambda/2$ and W L_α) arising from the Si 004, are marked by a *. (b) θ-2θ scan of the 004 film peak in which separate peaks from the *c*-axis oriented $BaTiO_3$ film ($2\theta \approx 99.6°$) and the $Ba_{0.7}Sr_{0.3}TiO_3$ buffer layer ($2\theta \approx 102°$) are clearly distinguishable. The out-of-plane lattice parameters of the $Ba_{0.7}Sr_{0.3}TiO_3$ and $BaTiO_3$ layers (from the 004 peak positions) are 3.960±0.001 and 4.025±0.003 Å, respectively. (c) ϕ-scan of the 111 $BaTiO_3/Ba_{0.7}Sr_{0.3}TiO_3$ peak with ϕ=0° aligned parallel to the [100] in-plane direction of the silicon substrate, showing that the film is epitaxial and oriented with a 45° in-plane rotation with respect to the silicon substrate. The FWHM in ϕ is 1.65°.

in Fig. 6. For a buffer layer thickness of 40 Å, the $Ba_{0.7}Sr_{0.3}TiO_3$ and $BaTiO_3$ peaks overlap, indicating that the $Ba_{0.7}Sr_{0.3}TiO_3$ layer is not completely relaxed and therefore, resulting in an *a*-axis oriented $BaTiO_3$ film. A double peak is barely discernable for a $Ba_{0.7}Sr_{0.3}TiO_3$ buffer layer thickness of 60 Å and gets more pronounced for thickness ⩾100 Å. The positions of the 004 $BaTiO_3$ peak at a 2θ value of ~99.6° and the 400 $Ba_{0.7}Sr_{0.3}TiO_3$ buffer layer peak at ~102.1° for buffer layer thicknesses of 100 and 300 Å indicate that the buffer layer is completely relaxed (no change in

Downloaded 05 Apr 2007 to 128.118.88.141. Redistribution subject to AIP license or copyright, see http://jap.aip.org/jap/copyright.jsp

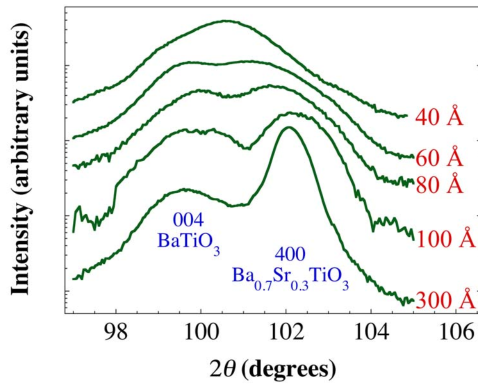

FIG. 6. (Color online) Comparison of the x-ray 004 peaks of $Ba_{0.7}Sr_{0.3}TiO_3$ and $BaTiO_3$ film on Si (001) as a function of $Ba_{0.7}Sr_{0.3}TiO_3$ buffer layer thickness (40–300 Å). The thickness of the $BaTiO_3$ layer on top of the $Ba_{0.7}Sr_{0.3}TiO_3$ buffer layer is ~80–100 Å.

lattice constant with increase in buffer layer thickness), which is an important part of our strategy to orient the *c*-axis of the tetragonal $BaTiO_3$ film out of plane.

The in-plane lattice constants were also measured to see if the $BaTiO_3$ film was commensurate with the $Ba_{0.7}Sr_{0.3}TiO_3$ buffer layer and to ascertain if the buffer layer itself is fully relaxed. This was accomplished by measuring the in-plane 200 peaks of the $Ba_{0.7}Sr_{0.3}TiO_3$ and $BaTiO_3$ layers by grazing-incidence diffraction on a synchrotron (the UNICAT beamline on the Advance Photon Source). These measurements indicated the 100-Å-thick $BaTiO_3$ film to be commensurate with the $Ba_{0.7}Sr_{0.3}TiO_3$ buffer layer and the buffer layer to be completely relaxed from the silicon substrate for thickness $\geqslant$100 Å. In Fig. 7, the in-plane 200 scan from a 200-Å-thick $Ba_{0.7}Sr_{0.3}TiO_3$/Si (001) is compared with the scan from a 100 Å $BaTiO_3$/300 Å $Ba_{0.7}Sr_{0.3}TiO_3$/Si (001) heterostructure. The peaks from both samples lie at the same 2θ value and have the same FWHM, showing the $BaTiO_3$ overlayer to be commensurate with the fully relaxed $Ba_{0.7}Sr_{0.3}TiO_3$ buffer layer. The in-plane lattice constant of $Ba_{0.7}Sr_{0.3}TiO_3$ and $BaTiO_3$ obtained from the synchrotron data is 3.9996±0.0005 Å.[53] The Si 220 peak (marked by * at 2θ=42.057°) is shown along with the film peak to illustrate that the buffer layer is completely relaxed from the substrate.

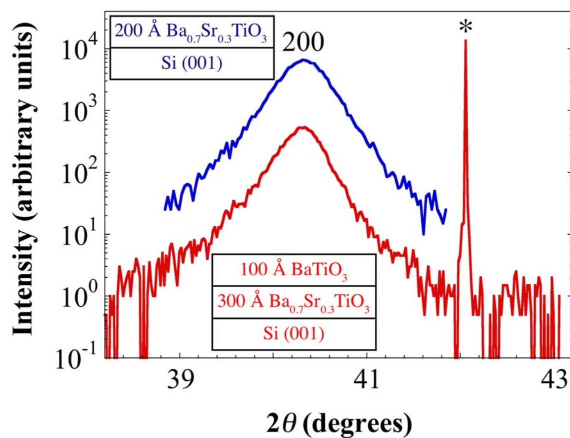

FIG. 7. (Color online) Synchrotron data showing the in-plane 200 peak of a $Ba_{0.7}Sr_{0.3}TiO_3$ buffer layer (300 Å thick), an overlying $BaTiO_3$ film (100 Å thick), and the 220 Si peak from the substrate. This is the same 100 Å $BaTiO_3$/300 Å $Ba_{0.7}Sr_{0.3}TiO_3$/Si (001) heterostructure whose RHEED patterns are shown in Fig. 4. The in-plane 200 peak of a relaxed $Ba_{0.7}Sr_{0.3}TiO_3$ film (200 Å thick) on Si (001) is shown for comparison. It is clear that the $Ba_{0.7}Sr_{0.3}TiO_3$ layer is completely relaxed and the $BaTiO_3$ layer is commensurately strained in-plane to the $Ba_{0.7}Sr_{0.3}TiO_3$ layer. The in-plane lattice constant of the $Ba_{0.7}Sr_{0.3}TiO_3$ and $BaTiO_3$ layer, obtained from the 200 peak, is 3.9996±0.0005 Å.

VI. SECOND HARMONIC GENERATION

The x-ray diffraction studies reveal that the $BaTiO_3$, in the 100 Å $BaTiO_3$/300 Å $Ba_{0.7}Sr_{0.3}TiO_3$/Si (001) oxide film heterostructure, is predominantly *c*-axis oriented. This conclusion was further corroborated by optical second harmonic generation (SHG) measurements. SHG involves the conversion of light at frequency ω into optical signal at a frequency of 2ω by the nonlinear material ($BaTiO_3$ film). The conversion process occurs by the creation of a nonlinear polarization $P_i^{2\omega} \propto d_{ijk} E_j^{\omega} E_k^{\omega}$, by light of frequency ω through the third order nonlinear tensor d_{ijk} (nonlinear optical coefficients). Each of the subscripts i, j, k refer to any one of the crystal physics axes of the material, 1, 2, 3. Both $BaTiO_3$ and $Ba_{0.7}Sr_{0.3}TiO_3$ have the point group symmetry of 4*mm*, where the four-fold rotation axis is also generally labeled as *c*, 3, and *z* axis. By symmetry considerations, the ferroelectric polarization, P_s in this point group can lie only along this four-fold axis, which is conventionally labeled as crystal physics axis 3. Additionally, by Neumann's law, only the nonlinear coefficients, d_{15}, d_{24}, $d_{31}=d_{32}$, and d_{33} are nonzero, where the abbreviated Voigt notation of $jk \rightarrow l$ is used.

From the d_{ij} tensor, one can generally conclude that for fundamental light (ω) propagating along the *c*-axis of $BaTiO_3$ or $Ba_{0.7}Sr_{0.3}TiO_3$, no SHG signal will be created in the direction of fundamental light propagation. A schematic of the reflection geometry used in the SHG experiments is shown in Fig. 8(a). One can therefore conclude that for light propagating perpendicular to the film surface, ($\varphi_i=\varphi_r=0°$), a film consisting of only *c* domains will *not* give rise to any SHG signal, while any signal observed will arise from a net contribution from the four types of *a* domains only. This fact alone does not allow us to distinguish the domain structure of the $Ba_{0.7}Sr_{0.3}TiO_3$ from the $BaTiO_3$ layers, since both have the same point group symmetry, and any SHG signal observed cannot be attributed to one or the other layer alone. Theory predicts, however, that the variation of the SHG intensity, $I^{2\omega}$, as a function of the incident angle φ_i should show a distinctly different signature for *c* domains and *a* domains as described below. For incident fundamental light polarized at an angle of θ to the incidence plane (*X*-*Z*), the *p-polarized* SHG intensity generated from purely *c* and *a* domains is given as

$$I_c^{2\omega} = K_{3c}(K_{1c}\cos^2\theta + K_{2c}\sin^2\theta)^2, \quad (c \text{ domains}), \qquad (2)$$

$$I_a^{2\omega} = K_{4a}(K_{1a}\cos^2\theta + K_{2a}\sin^2\theta + K_{3a}\sin 2\theta)^2, \quad (a \text{ domains}), \qquad (3)$$

where K_{ia} (i=1, 2, 3, and 4) and K_{ic} (i=1, 2, and 3) are constants that depend on nonlinear coefficients (d_{15}, d_{31}, and

Downloaded 05 Apr 2007 to 128.118.88.141. Redistribution subject to AIP license or copyright, see http://jap.aip.org/jap/copyright.jsp

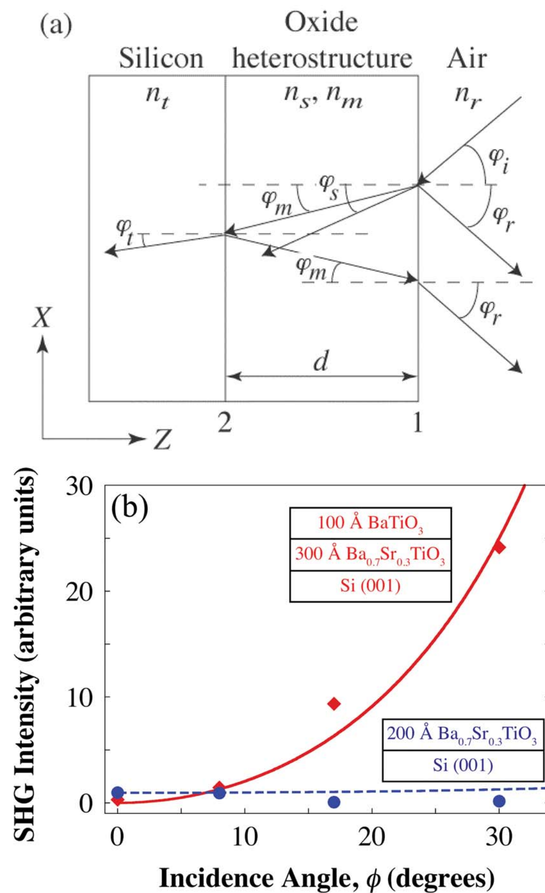

FIG. 8. (Color online) (a) Schematic of the SHG setup in reflection mode. The incident and SHG waves are shown using a section along the incident plane (*X-Z*). The three layers involved in the experiment are air, the oxide heterostructure, and the silicon substrate. The angles φ_m and φ_t and indices n_m and n_t correspond to SHG waves (frequency 2ω), the angles φ_s and φ_i and the index n_s correspond to fundamental wave (ω), and the angle φ_r and index n_r correspond to both SHG and fundamental waves. (b) SHG intensity of a *p*-polarized wave (polarization component parallel to the incident plane) as a function of incidence angle, shown as data points, from the same 100 Å $BaTiO_3$/300 Å $Ba_{0.7}Sr_{0.3}TiO_3$/Si (001) and 200 Å $Ba_{0.7}Sr_{0.3}TiO_3$/Si (001) heterostructures whose x-ray diffraction scans are shown in Fig. 7. Theoretical curves shown as continuous lines are calculated assuming that the $BaTiO_3$ layer in the 100 Å $BaTiO_3$/300 Å $Ba_{0.7}Sr_{0.3}TiO_3$/Si (001) is entirely *c*-axis oriented, while the $Ba_{0.7}Sr_{0.3}TiO_3$ layer in the 200 Å $Ba_{0.7}Sr_{0.3}TiO_3$/Si (001) is entirely *a*-axis oriented.

d_{33}), and the incidence angle φ_i through their dependence on linear Fresnel factors (t_x, t_y, and t_z) and nonlinear Fresnel factors (f_x, f_y, and f_z) describing the refraction of fundamental beam and second harmonic beam, respectively[54] (see Appendix for exact functional forms).

Calculated plots of $I_c^{2\omega}(\varphi_i)$ and $I_a^{2\omega}(\varphi_i)$ for $BaTiO_3$ thin films are shown in Fig. 8(b). One clearly observes that for pure *c* domains, the SHG intensity, $I_c^{2\omega}(\varphi_i)$, increases with a power law dependence on the incidence angle φ_i. On the other hand, the $I_a^{2\omega}(\varphi_i)$ arising from the *a* domains shows little change with increasing angle, φ_i. With these predictions in hand, SHG experiments were performed as follows: a fundamental wavelength (λ^{ω}) of 800 nm is incident with the geometry shown in Fig. 8(a), giving rise to SHG signal at a wavelength ($\lambda^{2\omega}$) of 400 nm. The incidence polarization is set to *p* polarized ($\theta=0°$) and the detected SHG polarization is also *p* polarized. The same oxide heterostructures characterized by RHEED and x-ray diffraction measurements (Figs. 4, 5, and 7) were investigated by SHG: 200 Å $Ba_{0.7}Sr_{0.3}TiO_3$/Si(001) and 100 Å $BaTiO_3$/300 Å $Ba_{0.7}Sr_{0.3}TiO_3$/Si(001). The experimental results, shown as data points, are overlayed with the theoretical predictions, shown as a continuous line, in Fig. 8(b). Excellent agreement between experiment and theory indicates that the 200 Å $Ba_{0.7}Sr_{0.3}TiO_3$ film on Si (001) is comprised of predominantly *a* domains, and the 100 Å $BaTiO_3$ film on 300 Å $Ba_{0.7}Sr_{0.3}TiO_3$/Si(001) is comprised of predominantly *c* domains, corroborating the x-ray diffraction studies.

VII. PIEZORESPONSE ATOMIC-FORCE MICROSCOPY

To further confirm the direction of film polarization as well as to check the ferroelectric nature of the $BaTiO_3$ films, experiments were performed to control the out-of-plane orientation of the spontaneous polarization using piezoelectric response (piezoresponse) atomic-force microscopy (AFM).[55–58] In this technique, an AFM is operated in contact mode while applying a small ac voltage (typically V_{ac} $=0.07$ V_{rms}) to a conductive cantilever. The electric field between the probe and the doped silicon substrate produces a small thickness change in the ferroelectric film, which is detected using a lock-in amplifier. Images of the piezoelectric response are obtained by scanning the sample over the conductive tip of the AFM cantilever. Piezoresponse measurements in noncontact mode for domain imaging and patterning have also been demonstrated.[57–60]

Experiments were performed using a Pt/Ti coated silicon cantilevers (Olympus AC-240TM) having a typical tip radius of 15 nm and a resonance frequency of 70 kHz in air. The frequency of the ac signal applied to the cantilever during scans was determined from a resonance curve obtained while in contact with the sample, prior to the start of patterning.

Domain patterning was accomplished programmatically, by selectively offsetting and biasing the AFM tip within the original scan region. Regular 3×3 grids of square, 400 nm domains, offset from one another by 700 nm, were written over 2.5×2.5 μm^2 regions of the 100 Å $BaTiO_3$/300 Å $Ba_{0.7}Sr_{0.3}TiO_3$/Si(001) sample. To normalize the background response of the film, the 2.5×2.5 μm^2 region was initially prepoled while scanning under a dc bias at −2 V. Following the prepoling, the 400 nm domains were written at 5 Hz, and the resulting domain pattern was imaged (256×256 points) using piezoresponse over the 2.5×2.5 μm^2 region centered on the pattern at 0.4 Hz. Figure 9 shows the piezoresponse for a set of domains written into this film (the same film characterized in Figs. 4–8) at a dc bias of +2 V on the AFM tip. The line profiles indicate the sharpness of the domain boundaries obtained. Subsequent experiments have confirmed the reversibility of the film polarization induced in this manner; out-of-plane oriented domains may be patterned controllably, erased, and reestablished in the same region of the 100 Å $BaTiO_3$/300 Å $Ba_{0.7}Sr_{0.3}TiO_3$/Si(001) ferroelectric heterostructure.

Downloaded 05 Apr 2007 to 128.118.88.141. Redistribution subject to AIP license or copyright, see http://jap.aip.org/jap/copyright.jsp

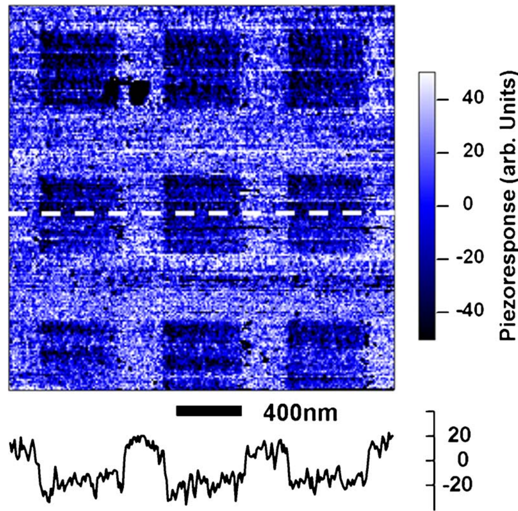

FIG. 9. (Color online) Ferroelectric domain patterns written on the same 100 Å $BaTiO_3$/300 Å $Ba_{0.7}Sr_{0.3}TiO_3$/Si (001) heterostructure whose RHEED and x-ray diffraction results are shown in Fig. 4–7 using piezoresponse AFM, corroborating the *c*-axis orientation of the $BaTiO_3$ film.

VIII. CONCLUSIONS

Using a relaxed $Ba_xSr_{1-x}TiO_3$ buffer layer, *c*-axis oriented epitaxial $BaTiO_3$ has been grown on (001) Si. X-ray measurements of the out-of-plane and in-plane lattice parameters validate a structural strategy that uses biaxial compressive epitaxial strain on a $BaTiO_3$ film to overcome the biaxial tensile strain from thermal expansion mismatch between the film and the substrate and, therefore, orient the *c*-axis of the $BaTiO_3$ film out of plane. SHG experiments on these heterostructures corroborate the presence of predominantly *c*-axis domains in the $BaTiO_3$ film. The out-of-plane spontaneous polarization in these films has been patterned with an AFM tip. These structures are an important enabler for devices on silicon requiring a ferroelectric layer with an out-of-plane spontaneous polarization.

ACKNOWLEDGMENTS

The authors gratefully acknowledge the financial support of DARPA QuIST through Contract No. DAAD-19-01-1-0650, the National Science Foundation through Grant Nos. DMR-0507146, DMR-0512165, and DMR-0349632, NSF-MRSEC center at Pennsylvania State University, and the MARCO, MSD Focus Center. The UNICAT facility at the Advanced Photon Source (APS) is supported by the U.S. DOE under Award No. DEFG02-91ER45439, through the Frederick Seitz Materials Research Laboratory at the University of Illinois at Urbana-Champaign, the Oak Ridge National Laboratory (U.S. DOE Contract No. DE-AC05-00OR22725 with UT-Battelle LLC), the National Institute of Standards and Technology (U.S. Department of Commerce) and UOP LLC. The APS is supported by the U.S. DOE, Basic Energy Sciences, Office of Science under Contract No. W-31-109-ENG-38.

APPENDIX

The constants K_{ic} and K_{ia} in Eqs. (2) and (3) are given by

$$K_{1c} = [-2d_{15}\alpha_x\alpha_z f_x + (d_{31}\alpha_x^2 + d_{33}\alpha_z^2)f_z], \tag{A1}$$

$$K_{2c} = (d_{31}\alpha_y^2 f_z), \tag{A2}$$

$$K_{3c} = \left[\frac{8\pi^2 d \sin\varphi_t^{2\omega}}{\lambda^{2\omega} n_r \sin(\varphi_i^{\omega} + \varphi_t^{2\omega})}\right]^2 \delta_{Z+/-}^2, \tag{A3}$$

$$K_{1a} = \delta_{X+/-}[(d_{33}\alpha_x^2 + d_{31}\alpha_z^2)f_x - (2d_{15}\alpha_x\alpha_z)f_z], \tag{A4}$$

$$K_{2a} = \delta_{X+/-}(d_{31}\alpha_y^2)f_x, \tag{A5}$$

$$K_{3a} = \delta_{Y+/-}d_{15}\alpha_y(\alpha_x f_x - \alpha_z f_z), \tag{A6}$$

and

$$K_{4a} = \left[\frac{8\pi^2 d \sin\varphi_t^{2\omega}}{\lambda^{2\omega} n_r \sin(\varphi_i^{\omega} + \varphi_t^{2\omega})}\right]^2, \tag{A7}$$

where, within a two-dimensional microstructure approximation, $\delta_{Z+/-}$ represents the difference in the area fraction of $+c$ domains to $-c$ domains, $\delta_{X+/-}$ represents the difference in the area fraction of $+X$ domains to $-X$ domains, and $\delta_{Y+/-}$ represents the difference in the area fraction of $+Y$ domains to $-Y$ domains. The coefficients α_x, α_y, and α_z have a linear relationship with the linear Fresnel factors (t_x, t_y, and t_z),

$$\alpha_x = t_x \cos\varphi_s^{\omega}, \quad \alpha_y = t_y, \quad \text{and } \alpha_z = t_z \sin\varphi_s^{\omega}. \tag{A8}$$

The linear and nonlinear Fresnel factors are given by[54]

$$\begin{pmatrix} t_x \\ t_y \\ t_z \end{pmatrix} = \frac{2\sin\varphi_s^{\omega}}{\sin(\varphi_i^{\omega} + \varphi_s^{\omega})}\left\{\begin{matrix} \cos\varphi_s^{\omega}/\cos(\varphi_s^{\omega} - \varphi_i^{\omega}) \\ \cos\varphi_s^{\omega} \\ (1/n_s^{\omega})[\cos\varphi_s^{\omega}/\cos(\varphi_s^{\omega} - \varphi_i^{\omega})] \end{matrix}\right\}, \tag{A9}$$

and

$$\begin{pmatrix} f_x \\ f_y \\ f_z \end{pmatrix} = \begin{pmatrix} -\cos\varphi_t^{2\omega}/\cos(\varphi_t^{2\omega} - \varphi_i^{\omega}) \\ 1 \\ (n_t^{2\omega}/n_m^{2\omega})^2(\sin\varphi_t^{2\omega}/\cos(\varphi_t^{2\omega} - \varphi_i^{\omega})) \end{pmatrix}. \tag{A10}$$

To simplify the SHG analysis, a single layer film of $BaTiO_3$ of thickness d on silicon was assumed in the above derivations. The interface index contrast between $BaTiO_3$ (n_e=2.32 and n_o=2.366 at a wavelength of 800 nm) (Ref. 61) and $Ba_{0.7}Sr_{0.3}TiO_3$ [n_o=2.358 (Ref. 62) at a wavelength of 800 nm, based on linear interpolation between the n_o values of $BaTiO_3$ and $SrTiO_3$ (Ref. 63)] is small and hence neglected. The refractive index of silicon is obtained from the *Landolt-Börnstein* tables.[64] Similarly, due to the lack of availability of data, the differences in the nonlinear coefficients d_{ij} between $BaTiO_3$ and $Ba_{0.7}Sr_{0.3}TiO_3$ are neglected. Nonlinear coefficients of d_{15}=+13.6, d_{31}=−14.4, and d_{33} =−5.5 pm/V were used for $BaTiO_3$.[65,66] Since the final aim of the work is not the absolute SHG intensity, but the variation of the SHG intensity with the incidence angle, φ_i, these assumptions were found to be acceptable for this study. As shown above, the *net* SHG intensity is also dependent on the relative area fractions of antiparallel domains in the probe region, which experimentally varies considerably from film to film, and with the location of the probe area within the

Downloaded 05 Apr 2007 to 128.118.88.141. Redistribution subject to AIP license or copyright, see http://jap.aip.org/jap/copyright.jsp

film. Hence the absolute SHG intensity is not relevant to this study. Therefore, the SHG intensity from Eqs. (2) and (3) are scaled accordingly to fit the experimental intensities in Fig. 8(b) to highlight the change in the functional form with increasing incident angle away from normal incidence ($\varphi_i = 0°$).

[1]A. I. Kingon, J.-P. Maria, and S. K. Streiffer, Nature (London) **406**, 1032 (2000).
[2]C. M. Hanson and H. R. Beratan, Proc. SPIE **4721**, 91 (2002.).
[3]D. Czekaj, Z. Surowiak, A. A. Bakirov, and V. P. Dudkievich, J. Eur. Ceram. Soc. **21**, 1609 (2001).
[4]E. Burcsu, G. Ravichandran, and K. Bhattacharya, Appl. Phys. Lett. **77**, 1698 (2000).
[5]K. Abe, N. Yanase, S. Komatsu, K. Sano, N. Fukushima, and T. Kawakubo, IEICE Trans. Electron. **E81-C**, 505 (1998).
[6]P. Tang, D. J. Towner, T. Hamano, A. L. Meier, and B. W. Wessels, Opt. Express **12**, 5962 (2004).
[7]A. Petraru, J. Schubert, M. Schmid, and Ch. Buchal, Appl. Phys. Lett. **81**, 1375 (2002).
[8]B. W. Wessels, J. Cryst. Growth **195**, 706 (1998).
[9]S. Miura, T. Yoshitake, S. Matsubara, Y. Miyasaka, N. Shohata, and T. Satoh, Appl. Phys. Lett. **53**, 1967 (1988).
[10]D. K. Fork, F. A. Ponce, J. C. Tramontana, and T. H. Geballe, Appl. Phys. Lett. **58**, 2294 (1991).
[11]R. A. McKee, F. J. Walker, J. R. Conner, E. D. Specht, and D. E. Zelmon, Appl. Phys. Lett. **59**, 782 (1991).
[12]Z. Yu, J. Ramdani, J. A. Curless, C. D. Overgaard, J. M. Finder, R. Droopad, K. W. Eisenbeiser, J. A. Hallmark, W. J. Ooms, and V. S. Kaushik, J. Vac. Sci. Technol. B **18**, 2139 (2000).
[13]M.-B. Lee, M. Kawasaki, M. Yoshimoto, and H. Koinuma, Appl. Phys. Lett. **66**, 1331 (1995).
[14]J. W. Matthews, in *Epitaxial Growth, Part B*, edited by J. W. Matthews (Academic, New York, 1975), pp. 559–609.
[15]D. Taylor, Br. Ceram. Trans. J. **84**, 181 (1985).
[16]*Landolt-Börnstein: Numerical Data and Functional Relationships in Science and Technology*, New Series, Group III, Vol. 22, Pt. A, edited by O. Madelung (Springer, Berlin, 1987), p. 18.
[17]*Landolt-Börnstein: Numerical Data and Functional Relationships in Science and Technology*, New Series, Group III, Vol. 16, Pt. A, edited by K.-H. Hellwege and A. M. Hellwege (Springer, Berlin, 1981), p. 67.
[18]R. A. McKee and F. J. Walker, U.S. Patent No. 6, 103,008 (15 August 2000).
[19]J. M. Pond, S. W. Kirchoefer, W. Chang, J. S. Horwitz, and D. B. Chrisey, Integr. Ferroelectr. **22**, 317 (1998).
[20]O. Auciello, J. F. Scott, and R. Ramesh, Phys. Today **51**(7), 22 (July 1998).
[21]J. Levy, Phys. Rev. A **64**, 052306 (2001).
[22]J. S. Speck and W. Pompe, J. Appl. Phys. **76**, 466 (1994).
[23]N. A. Pertsev, A. G. Zembilgotov, and A. K. Tagantsev, Phys. Rev. Lett. **80**, 1988 (1998).
[24]Y. L. Li, S. Y. Hu, Z. K. Liu, and L. Q. Chen, Appl. Phys. Lett. **78**, 3878 (2001).
[25]Y. L. Li, L. E. Cross, and L. Q. Chen, J. Appl. Phys. **98**, 064101 (2005).
[26]Y. L. Li and L. Q. Chen, Appl. Phys. Lett. **88**, 072905 (2006).
[27]J. S. Speck, A. Seifert, W. Pompe, and R. Ramesh, J. Appl. Phys. **76**, 477 (1994).
[28]W. J. Lin, T. Y. Tseng, H. B. Lu, S. L. Tu, S. J. Yang, and I. N. Lin, J. Appl. Phys. **77**, 6466 (1995).
[29]R. A. McKee and F. J. Walker, U.S. Patent No. 6, 080,235 (27 June 2000).
[30]R. A. McKee and F. J. Walker, U.S. Patent No. 5, 482,003 (9 January 1996).
[31]L. Vegard, Z. Phys. **5**, 17 (1921).
[32]L. Vegard, Z. Phys. **67**, 239 (1928).
[33]J. W. Matthews, S. Mader, and T. B. Light, J. Appl. Phys. **41**, 3800 (1970).
[34]J. W. Matthews and A. E. Blakeslee, J. Cryst. Growth **27**, 118 (1974).
[35]T. Suzuki, Y. Nishi, and M. Fujimoto, Philos. Mag. A **79**, 2461 (1999).
[36]E. J. Huibregtse, W. H. Bessey, and M. E. Drougard, J. Appl. Phys. **30**, 899 (1959).
[37]S. P. Alpay, I. B. Misirlioglu, A. Sharma, and Z.-G. Ban, J. Appl. Phys. **95**, 8118 (2004).
[38]The strain due to thermal expansion mismatch between the silicon substrate and $BaTiO_3$ film is calculated by assuming an equivalent cubic cell of the same volume as tetragonal $BaTiO_3$ at temperatures below the bulk Curie temperature of $BaTiO_3$.
[39]J. Lettieri, J. H. Haeni, and D. G. Schlom, J. Vac. Sci. Technol. A **20**, 1332 (2002).
[40]J. Lettieri, Ph.D. thesis, Pennsylvania State University, 2002; available online at http://etda.libraries.psu.edu/theses/approved/WorldWideIndex/ETD-202/index.html
[41]V. Vaithyanathan, J. Lettieri, J. Haeni, J. Schubert, and D. G. Schlom (unpublished).
[42]F. J. Walker and R. A. McKee, in *High Dielectric Constant Materials: VLSI MOSFET Applications*, edited by H. R. Huff and D. C. Gilmer (Springer, Berlin, 2005), pp. 607–637.
[43]S. Jeon, F. J. Walker, C. A. Billman, R. A. McKee, and H. Hwang, IEEE Electron Device Lett. **24**, 218 (2003).
[44]J. Lettieri, L. F. Edge, V. Vaithyanathan, J. Rodríguez Contreras, and D. G. Schlom (unpublished).
[45]1 ML is defined as the concentration of atoms on the (001) surface of silicon, i.e., 6.78×10^{14} atoms/cm^2.
[46]Y. Liang, S. Gan, and M. Engelhard, Appl. Phys. Lett. **79**, 3591 (2001).
[47]The commensurate nature of (Ba,Sr)O films displaying such ideal RHEED patterns was confirmed by four-circle x-ray diffraction (the films were capped with aluminum to prevent degradation in air when removed from the MBE chamber).
[48]M. G. Lagally, D. E. Savage, and M. C. Tringides, in *Reflection High-Energy Electron Diffraction and Reflection Electron Imaging of Surfaces*, edited by P. K. Larsen and P. J. Dobson (Plenum, New York, 1988), Vol. 188, pp. 139–174.
[49]J. Lettieri, J. H. Haeni, D. G. Schlom, B. T. Liu, K. Maki, Y. So, V. Nagarajan, R. Ramesh, W. Tian, and X. Q. Pan, presented at the 44th Electronic Materials Conference, Santa Barbara, CA, 2002 (unpublished).
[50]G. Springholz and G. Bauer, Phys. Rev. B **48**, 10998 (1993).
[51]J. H. Haeni, C. D. Theis, and D. G. Schlom, J. Electroceram. **4**, 385 (2000).
[52]It is not possible to distinguish whether the structural distortion of $Ba_{0.7}Sr_{0.3}TiO_3$ buffer layer is due to thermal expansion mismatch induced tensile strain or due to strain-induced paraelectric-ferroelectric (or cubic-tetragonal) phase transition. Therefore, pseudocubic indexing of the $Ba_{0.7}Sr_{0.3}TiO_3$ buffer layer is used throughout this manuscript.
[53]The in-plane lattice spacing and therefore the lattice constant of the film are obtained from the synchrotron data using the following equation, $d_{film} \sin \theta_{film} = d_{sub} \sin \theta_{sub}$ (variation of Bragg's law) and the known lattice spacing of the substrate (silicon, in our case). d_{film} and d_{sub} are the lattice spacings of the film and substrate (silicon), respectively, and θ_{film} and θ_{sub} are the Bragg peak positions (established using a Gaussian fit of the synchrotron data) of the film peak and substrate reference peak (Si 220), respectively.
[54]B. Dick, A. Gierulski, G. Marowsky, and G. A. Reider, Appl. Phys. B: Photophys. Laser Chem. **38**, 107 (1985).
[55]A. Gruverman, O. Auciello, and H. Tokumoto, Annu. Rev. Mater. Sci. **28**, 101 (1998).
[56]C. S. Ganpule, V. Nagarajan, H. Li, A. S. Ogale, D. E. Steinhauer, S. Aggarwal, E. Williams, R. Ramesh, and P. De Wolf, Appl. Phys. Lett. **77**, 292 (2000).
[57]C. H. Ahn, K. M. Rabe, and J.-M. Triscone, Science **303**, 488 (2004).
[58]P. Güthner and K. Dransfeld, Appl. Phys. Lett. **61**, 1137 (1992).
[59]C. H. Ahn, T. Tybell, L. Antognazza, K. Char, R. H. Hammond, M. R. Beasley, Ø. Fischer, and J.-M. Triscone, Science **276**, 1100 (1997).
[60]F. Saurenbach and B. D. Terris, Appl. Phys. Lett. **56**, 1703 (1990).
[61]*Landolt-Börnstein: Numerical Data and Functional Relationships in Science and Technology*, New Series, Group III, Vol. 36, Pt. A., edited by Y. Shiozaki, E. Nakamura, and T. Mitsui (Springer, Berlin, 2002), p. 22.
[62]In bulk, $Ba_{0.7}Sr_{0.3}TiO_3$ is cubic at room temperature and hence has isotropic refractive index.
[63]W. L. Bond, J. Appl. Phys. **36**, 1674 (1965).
[64]*Landolt-Börnstein: Numerical Data and Functional Relationships in Science and Technology*, New Series, Group III, Vol. 41 Pt. A1, edited by U. Rössler (Springer, Berlin, 2001).
[65]R. C. Miller and W. A. Nordland, Phys. Rev. B **2**, 4896 (1970).
[66]R. C. Miller, D. A. Kleinman, and A. Savage, Phys. Rev. Lett. **11**, 146 (1963).

Downloaded 05 Apr 2007 to 128.118.88.141. Redistribution subject to AIP license or copyright, see http://jap.aip.org/jap/copyright.jsp